Pergamon

PII: S0301-9322(96)00079-1

Int. J. Multiphase Flow Vol. 23, No. 3, pp. 561–574, 1997

Printed in Great Britain
0301-9322/97 $17.00 + 0.00

A NOTE ON INERTIAL EFFECTS IN THE DEFORMATION OF NEWTONIAN DROPS IN A UNIAXIAL EXTENSIONAL FLOW

S. RAMASWAMY and L. G. LEAL

Department of Chemical Engineering, University of California, Santa Barbara, CA 93016, U.S.A.

(Received 10 September 1995; in revised form 21 October 1996)

Abstract—We consider inertial effects, for Reynolds numbers in the range $1 \leqslant \mathrm{Re} \leqslant 300$, on the deformation of a Newtonian drop in a steady, uniaxial extensional flow. Previous studies of a deformable bubble have demonstrated that there is a qualitative change in the nature of the shape as the dominant stresses at the interface go from viscous to dynamic pressure with increase of Reynolds number. In the present paper, we focus on the effects of finite viscosity and density of the interior fluid. © 1997 Elsevier Science Ltd. All rights reserved.

Key Words: extensional flows, drops, deformation, density ratio, viscosity ratio, inertial effects

1. INTRODUCTION

The present paper reports on a computational study of inertial effects on the deformation of a drop that is subjected to a uniaxial extensional flow. There has been considerable interest for many years in the deformation and breakup of liquid drops immersed in linear shear or extensional flow of a second immiscible fluid.

For the most part, these works have followed the lead of the early pioneering study of Taylor (1934), and focused upon the *Stokes flow* limit for drops that are density-matched to the surrounding fluid. Although many applications involve considerably higher Reynolds numbers, relatively little theoretical work has been done to assess inertial effects at finite or large Reynolds numbers. One noteworthy exception was reported by Dandy and Leal (1989) who numerically studied the buoyancy driven motion of a deformable drop in an unbounded fluid at moderate Reynolds numbers, 1–300.

The work most closely related to that reported here was a series of studies by Ryskin and Leal (1984a) and Kang and Leal (1987, 1989) who considered both steady and transient deformation of an incompressible *bubble* (perhaps better described as a drop in the limit of vanishing material viscosity and density) for a series of steady and time-dependent uniaxial extensional flows. Since the objective was to understand deformation and breakup processes due to an imposed velocity gradient, gravitational effects were neglected, as they had been in all of the low Reynolds number studies. It was shown, in these earlier studies, that the qualitative nature of the bubble deformation in extensional flow is very different at high and low Reynolds numbers. In the latter case, as the capillary or Weber number is increased, the bubble elongates and develops shapes with relatively high curvature at the ends. However, as Reynolds number increases, the deformation is increasingly caused by gradients in the dynamic pressure at the bubble surface. Since the dynamic pressure is highest at the two ends and at the equator where there are stagnation points, the bubble becomes more barrel-like in shape with flattened ends and a cylindrical shape near the equator.

In this paper, we present numerical solutions for the deformation of a Newtonian *drop* in a uniaxial extensional flow at finite/large Reynolds numbers. Our primary goal is to elucidate the effect of the inner fluid on the drop shape, in a regime of parameter space where the dominant contribution to the drop shape is due to variations of the dynamic pressure at the surface of the drop. Unlike the 'bubble' limit considered earlier, where the density ratio, $\zeta = \hat{\rho}/\rho$, between the

inner and outer fluid was assumed to be zero so that the only dynamic pressure contributions came from the outer fluid, we consider finite values of ζ where there are significant dynamic pressure variations also in the interior of the drop. Since the interior flow has stagnation points at the same positions on the interface as the exterior fluid, the tendency of the pressure maxima in the outer fluid to produce shortened, barrel-like shapes will be compensated (or perhaps even dominated) by the pressure maxima in the inner fluid.

In the limit as $\mathrm{Re} \to \infty$, we would expect the solution to consist of an inviscid, potential flow in the exterior fluid, and an inviscid rotational flow inside the drop satisfying the Prandtl–Batchelor theorem, with the exception of thin boundary-layers at the interface and along the central symmetry plane inside. Hence the shape should become a function only of the Weber number and the density ratio, with the changes due to finite values of the Reynolds number or variations in the viscosity ratio appearing as small corrections. We shall see to what extent these expectations are realized in the range of Reynolds numbers up to 300 considered here.

We recognize, of course, that gravitational effects cannot generally be neglected in the presence of a finite density difference. The one obvious exception is micro-gravity applications: e.g. containerless processing of materials as levitated drops (Doremus and Nordine 1986; Lai 1990; Barmatz 1982; Wozniak 1991). The fact is, however, that gravitational effects have been neglected in all prior analysis of drop deformation in shear or extensional flows, both at high and low Reynolds number. The only 'justification' outside the microgravity arena, is that the result is a radically simpler problem from which to begin to understand the effects of velocity gradients on flow-induced deformation and breakup processes. Because one solution in the creeping flow limit for the shape of a buoyancy-driven drop in a quiescent fluid is a sphere, it might seem at first that the deformation due to a mean velocity gradient in the exterior fluid should be the same, whether the buoyancy driven motion is included or not, thus justifying the neglect of gravitational effect at low Reynolds number in a way that is not possible for the finite Reynolds number cases considered here. However, this is not actually true. Koh and Leal (1972) has shown that the translational motion can induce very significant deformations of shape in the creeping flow limit if the drop is initially deformed (essentially, the solution for drop shape is not unique, but depends on initial conditions). Hence, with a non–spherical state created by the shear or extensional flow, the addition of a buoyancy-driven translational motion produces an inseparable non-linear coupling effect on the drop shape, even in the creeping flow limit. Thus, to properly investigate the effect of buoyancy in a shear or extensional flow, at any Reynolds number, we would need to consider all possible combinations of the orientation of the axis of symmetry of the shear or extensional flow and the gravitational vector. This is clearly impossible from a practical point of view and it is this fact which has led everyone who has studied velocity gradient induced breakup to consider only the idealized problem in which buoyancy is neglected entirely. Although the results are directly applicable in a technological sense only in the micro-gravity limit mentioned earlier, we believe that our results provide useful fundamental insights into the role of inertial effects that would be obscured by inclusion of buoyancy driven motions, in much the same way that earlier studies at low Reynolds number elucidated the role of viscous stresses in drop deformation and breakup

2. PROBLEM STATEMENT

We consider the deformation of a Newtonian drop of volume $\frac{4}{3}\pi a^3$, constant viscosity and density, $\hat{\mu}$ and $\hat{\rho}$, subjected to a steady uniaxial extensional flow of a fluid with constant density ρ and constant viscosity μ. The interface is characterized by a uniform surface tension coefficient γ.

This axisymmetric problem can be conveniently represented in terms of a cylindrical coordinate system (z, σ, ϕ), in which the axis of symmetry is coincident with the z coordinate axis. Due to the symmetry of the problem, it is necessary only to solve for the flow in one quadrant of the drop.

The velocity field far from the drop is given by

$$\mathbf{u} = \mathbf{E}\cdot\mathbf{r}, \tag{1}$$

where

$$\mathbf{E} = E\begin{bmatrix} -\frac{1}{2} & 0 & 0 \\ 0 & -\frac{1}{2} & 0 \\ 0 & 0 & 1 \end{bmatrix}$$

and E is the principal strain rate.

The governing equations, both inside and outside the drop are the Navier–Stokes and continuity equations. If we non-dimensionalize them using the undeformed drop radius a as a characteristic length scale, the product (Ea) as a characteristic velocity and $\frac{1}{2}\rho(Ea)^2$ as a characteristic pressure, they take the form

$$\nabla\cdot\hat{\mathbf{u}} = \mathbf{0}, \tag{2}$$

$$\hat{\mathbf{u}}\cdot\nabla\hat{\mathbf{u}} = -\frac{1}{2\zeta}\nabla\hat{p} + \frac{2\lambda}{\zeta\mathrm{Re}}\nabla^2\hat{\mathbf{u}} \tag{3}$$

inside the drop, and

$$\nabla\cdot\mathbf{u} = \mathbf{0}, \tag{4}$$

$$\mathbf{u}\cdot\nabla\mathbf{u} = -\frac{1}{2}\nabla p + \frac{2}{\mathrm{Re}}\nabla^2\mathbf{u} \tag{5}$$

for the suspending fluid. The dimensionless parameters that appear in these equations are the Reynolds number

$$\mathrm{Re} \equiv 2a\rho(Ea)/\mu$$

the density ratio $\zeta \equiv \hat{\rho}/\rho$, the viscosity ratio $\lambda \equiv \hat{\mu}/\mu$ and the internal Reynolds number

$$\hat{\mathrm{Re}} \equiv \mathrm{Re}\zeta/\lambda.$$

In addition to the far-field condition [1], the non-dimensionalized boundary conditions at the drop surface are continuity of velocity

$$\hat{\mathbf{u}} = \mathbf{u}, \tag{6}$$

the kinematic condition for a drop of fixed shape

$$\mathbf{n}\cdot\hat{\mathbf{u}} = \mathbf{n}\cdot\mathbf{u} = \mathbf{0} \tag{7}$$

and continuity of normal stress

$$\mathbf{n}\cdot(\mathbf{T} - \hat{\mathbf{T}}) = \frac{4}{\mathrm{We}}(\nabla\cdot\mathbf{n})\mathbf{n}. \tag{8}$$

The dimensionless group that appears in [8] is the Weber number, defined as $\mathrm{We} \equiv 2\rho(Ea)^2a/\gamma$. $\mathbf{T}$ and $\hat{\mathbf{T}}$ refer to the dimensionless stress tensors for the outer and inner fluids, respectively, and are defined as

$$\mathbf{T} = -p\mathbf{I} + \frac{8}{\mathrm{Re}}\tau$$

$$\hat{\mathbf{T}} = -\hat{p}\mathbf{I} + \frac{8}{\mathrm{Re}}\lambda\hat{\tau}.$$

The tangential stress balance takes the form of a condition relating the internal and external vorticities at the surface of the drop. We solve the free-boundary problem posed above using the same numerical technique that was developed by Dandy and Leal (1989) for the problem of uniform flow past a deformable drop at large Reynolds numbers. Since the technique was described in detail in the earlier paper (Dandy and Leal 1989), we do not describe it here except to say that it is a finite difference method, implemented on a numerically generated boundary-fitted

orthogonal coordinate system, both inside and outside the drop. The calculations were mainly carried out using the Cray Y-MP at the San Diego Supercomputer Center.

3. RESULTS

The primary objective of the present study is to determine the changes in the relationship between drop shape and Re, as we vary ζ and λ from the limiting values of zero that were considered earlier (Ryskin and Leal 1984b) to finite values. Since we already know the behavior of the drop for $\zeta = \lambda = 0$ (Ryskin and Leal 1983), we only consider ζ and λ values that are greater than or equal to one.

As in the previous study (Ryskin and Leal 1984b), we found that steady solutions could not be obtained beyond certain parameter values. Based on our earlier work, we believe that these critical conditions represent true limit points for the branch of steady solutions (Kang and Leal 1987).

3.1. Tests of numerical accuracy

As a check on the present code, we first compared our results with the results for a bubble as found by Kang and Leal (1987). First for Re = 10, We = 0.8, we set $\lambda = 10^{-8}$ and $\zeta = 10^{-8}$. Our results for the shape compared exactly ($O(10^{-6})$) with the results for a bubble. The maximum norm of the error for the stream-function was 10^{-4} and for the vorticity it was 10^{-5}. In addition, we compared the drop shape for Re = 100, We = 2.0, $\lambda = 10^{-10}$ and $\zeta = 10^{-10}$ with the result for a bubble at the same Re and We. There was again excellent agreement. In particular, the scalar deformation parameter D_f agreed to within 10^{-3} and the vorticity and stream-function agreed to within 10^{-4} (see figure 1).

In figure 2 we show the deformation as a function of Weber number for Re = 100 using inner and outer grids that each have 41 × 41, 51 × 51, 61 × 61, 71 × 71 points. We can see that there is very good agreement at low deformations for all cases. The only slight differences occur at the higher We. The inset graph shows a blowup view of the change in D_f with change in the level of discretization for We = 1.5. We can see that the results for D_f converge as we move from the 41 × 41 grid to the 71 × 71 grid with the change from 61 × 61 to 71 × 71 being small. On the basis of these and similar results at other elected values of Re, we used a 61 × 61 grid for both the outer and inner domains for all of the calculations reported here.

To establish convergence for each run, we checked the normal stress balance at the interface. A difference in the normal stress balance equal to (or smaller than) $O(10^{-3})$, was assumed to be converged. We also checked the velocity continuity condition at the interface. The velocity mismatch at the interface converged to within 0.0001 and usually evolved faster than the normal stress balance. When these two convergence criteria were met, the maximum norm of the error in the governing equations was found to be of $O(10^{-3})$ for all cases.

Let us now look at the influence of the parameters λ, ζ and We at various Reynolds numbers.

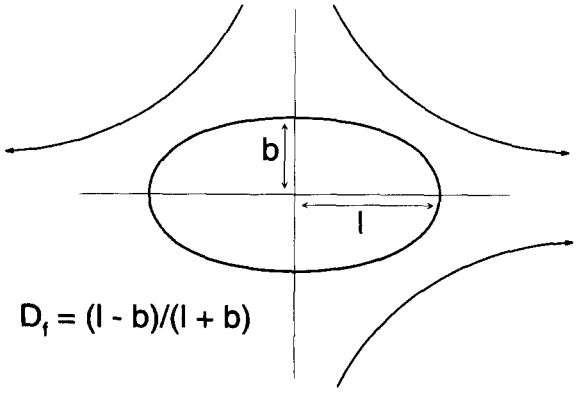

Figure 1. Drop in an axisymmetric extensional flow.

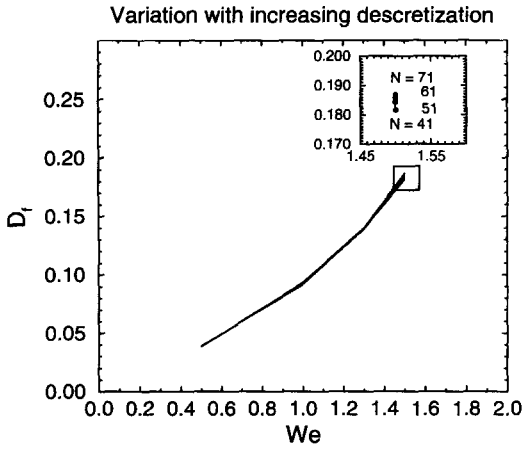

Figure 2. Drop deformation vs Weber number for a Reynolds number of 100; $\lambda = \zeta = 1$. Results are shown at four different mesh discretization levels from 41 × 41 to 71 × 71.

3.2. *Results for* Re = 1.0

We begin with a relatively small values of Re = 1.0. Figure 3 illustrates the qualitative nature of the changes in drop shape with increasing Weber number for three different value of the viscosity ratio. In addition, the drop deformation results obtained by Stone and Leal (1989) for Re = 0, $\lambda = 1.0$ are also included by way of comparison. Our results for Re = 1 show the same general low Reynolds number pattern of deformation that was first seen in the creeping flow limit by Stone and Leal (1989), with the drop becoming significantly elongated prior to breakup. Though the drop shapes shown explicitly in figure 3 are for $\lambda = 0.1$, they are representative of the general nature of the deformation at this Re. In general, we find that at a constant We, the deformation increases with increasing λ, as is also true in the creeping flow limit (Stone and Leal 1989). With We incremented in intervals of 0.01, the last point for each curve in figure 3 is the largest value of We for which steady solution was obtained. The corresponding critical Weber numbers appear to be We = 0.16, 0.12, 0.09 for $\lambda = 0.1$, 1 and 10. Another way of interpreting our results is that for each We $\geqslant 0.09$, there exists a critical value of λ above which a stable drop shape does not exist. The minimum We where this is true corresponds to the critical We for the limit $\lambda \rightarrow \infty$. Although we have not carried out calculations for $\lambda \geqslant 10$, we expect the results to become insensitive to λ for $\lambda \geqslant 10$ and thus the estimate $(\mathrm{We_{crit}})_{\min} \approx 0.09$ may not be too far above the actual limiting value. In addition, it is worth mentioning that Ryskin and Leal (1984b) found the critical Weber number for a bubble ($\lambda = 0$) at Re = 1 to be We = 0.25 with a

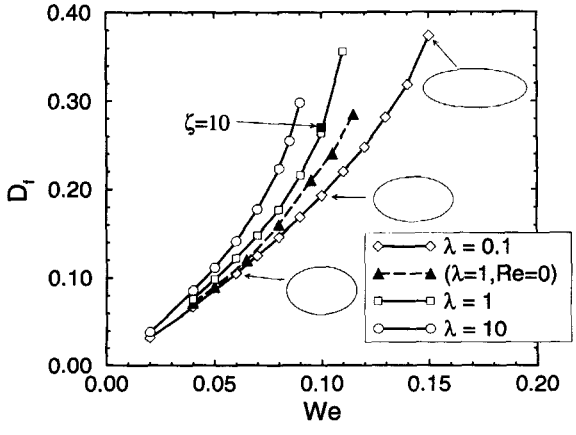

Figure 3. Drop deformation vs Weber number for Re = 1 and $\zeta = 1$ at three different viscosity ratios: ◇ $\lambda = 0.1$; □ $\lambda = 1.0$; ○ $\lambda = 10$. Also shown is the result from Stone and Leal (1989) for $\lambda = 1$ and Re = 0. Drop shapes are shown at three values of We for the case $\lambda = 0.1$.

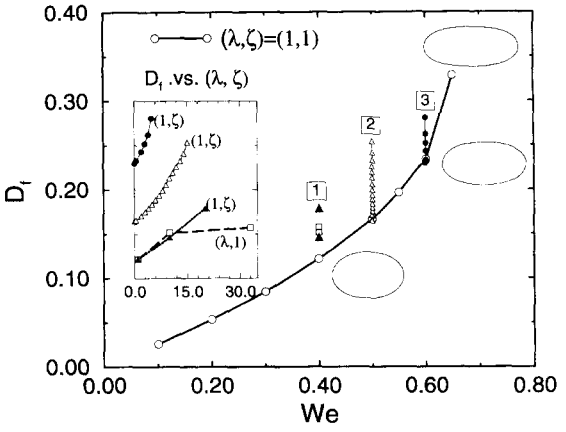

Figure 4. Drop deformation vs Weber number for Re = 10. The main curve ○—○ shows results for $\lambda = \zeta = 1$. The vertical set of points labelled 2 and 3, respectively, represent results for various values of $\zeta > 1$ and $\lambda = 1$ at We = 0.5 and 0.6. The set labelled 1 contains results for We = 0.4 at both $\zeta > 1$, $\lambda = 1$; and $\lambda > 1$, $\zeta = 1$. The details of the sets 1–3 are shown in the inset where we plot D_f vs either ζ or λ for the three fixed values of We.

corresponding maximum steady deformation, $D_f = 0.4$. This seems to be consistent with the results shown in figure 3.

We can also compare our results with the creeping flow solutions of Stone and Leal (1989). Though only the creeping flow results for $\lambda = 1$ is shown in figure 3, the same pattern was found for $\lambda = 0.1$, 10. It can be seen that the degree of deformation for any value of Ca = We/Re is increased relative to the solutions at Re = 0. Ryskin and Leal (1984b) found a similar result for the deformation of a bubble in an extensional flow, and the slender-body analysis of Arivos and Lo for $\lambda \ll 1$ also shows slightly increased deformation upon the inclusion of inertia.

At this Re, the viscosity ratio is the major factor in addition to We which influences deformation. For example, an increase in the density ratio from $\zeta = 1$ to 10 with We = 0.1, $\lambda = 1$ (figure 3), only changed the deformation measure by 0.01, a very small effect compared to the influence of λ.

3.3. *Results for* Re = *10.0*

Results for Re = 10 are shown in figure 4, including pictures of the drop shape for $\lambda = \zeta = 1$ at several values of We. Careful comparison with the results of figure 3 shows the first signs of a qualitative change in the drop shape. In particular, it is evident that the higher Reynolds number drop is less elongated and also more barrel shaped. We also see that the critical Weber number for breakup with $\lambda = \zeta = 1$ has gone up from We = 0.12 to We = 0.63.

We have also included results in figure 4 for a number of values of $(\lambda, \zeta) > 1$, in order to illustrate the effect of these parameters in the deformation (see inset graph). We see that, We = 0.4, the deformation increases with λ (at $\zeta = 1$), up to $\lambda = 10$ but then becomes fairly insensitive to further increase of λ.

If we compare the influence of λ for cases at Re = 1 and Re = 10 which have the same D_f at $\lambda = 1$, we find that the sensitivity to changes in λ appears to be of the same order in both cases. For example, the change in D_f as λ is increased from 1 to 10 is essentially equal for Re = 1, We = 0.06 (figure 3) and Re = 10, We = 0.4, where $D_f \approx 0.11$ in both cases for $\lambda = 1$. We can also see from figure 4 that the density ratio now plays a significant role, with an increase in ζ yielding a significant increase in the deformation. The details of changes in D_f with increase of ζ are shown in the insert of figure 4 for the three cases marked as 1–3. As the internal density is increased, the importance of the variations of the internal pressures also increases. At the crudest level of approximation, the stagnation pressure at the axis of symmetry inside the drop compensates for that outside and the drop elongates.

For Re = 10, the critical We at $\lambda = 1$, $\zeta = 1$ is approximately 0.63. Ryskin and Leal (1984b) later Kang and Leal (1987) determined the critical We for bubbles ($\lambda = 0$) to be 0.9. The solutions above, show that deformation increases with increase in and ζ for a fixed We number.

Thus we expect that the critical We should decrease with increase in the viscosity and density ratios but we have not explored this point in detail for this particular Re.

3.4. *Results for* Re = *100, 200, 300*

Finally, we have carried out a fairly large set of computations at Reynolds numbers of 100, 200 and 300. In many regards, the results for these three cases are similar, reflecting the transition to a range of Reynolds numbers where both the fluid dynamics and the drop shape are dominated by inertial effects. Thus in the first part of this section, we shall focus primarily on the case Re = 100, where the most extensive results are available. Later, we shall discuss the role of Re in some detail.

We begin by considering the effects of changes in ζ and λ from a qualitative point of view. For this purpose, we show in figure 5 the shapes of drops for Re = 100, for two values of $\lambda(=1$ and 10) and various values of We and ζ, including the largest We $\approx$ $\mathrm{We}_{\mathrm{critical}}$ in each case. In addition, the shapes for three cases with $\zeta = \lambda = 0$ are reproduced from earlier works of Ryskin and Leal (1984b). The most obvious trend, apart from increased deformation with increased We, is that the degree of drop elongation increases with increase in the density of the interior fluid. The bubble pictured at We = 2.1 was the maximum steady deformation achieved in the study of Ryskin and Leal (1984b). Subsequent studies of transient deformation due to Kang and Leal (1989) showed that this case corresponded very closely to a true limit point for the existence of steady solutions. With increased internal density, the critical We decreases, at least for $\lambda = O(1)$, and the final drop shapes shown in the last column of figure 5 for $\zeta = 0.1$, We = 1.8 and $\zeta = 1$, We = 1.63 are both close to the maximum We for existence of a steady state at these respective values of ζ for $\lambda = 1$. Not only can one see that the critical We is decreased with increase of ζ, but also that the drop shape is sufficiently modified that the final steady-state degree of deformation is substantially increased.

It was shown in previous studies that an apparent geometric condition signalling the failure of steady solutions and the onset of time-dependent deformation (leading to breakup), was that the curvature of the drop (or bubble) interface parallel to the symmetry axis changes sign from positive (concave) to negative (convex) at the central plane of symmetry, i.e. the drop forms a 'waist'. We have noted earlier, that the expected influence of an increase in the internal density (i.e. the density ratio) is to produce increased dynamic pressures in the inner fluid at the interface, with the maxima at the stagnation points at the axis of symmetry and at the central symmetry plane. The internal

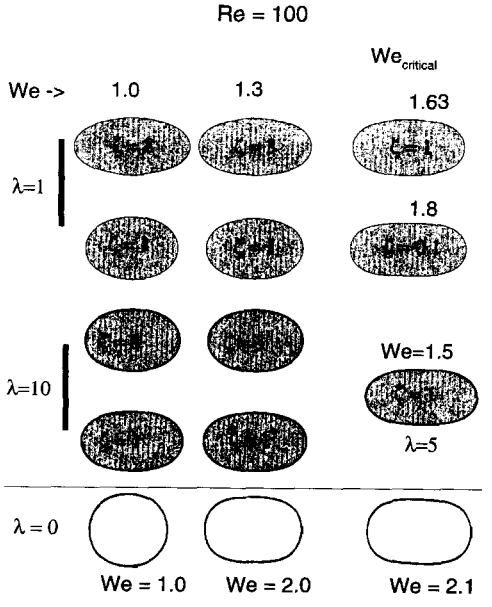

Figure 5. Drop shapes for Re = 100 at various values of λ, ζ and We. The results for $\lambda = 0$ are reproduced from Ryskin and Leal (1984b).

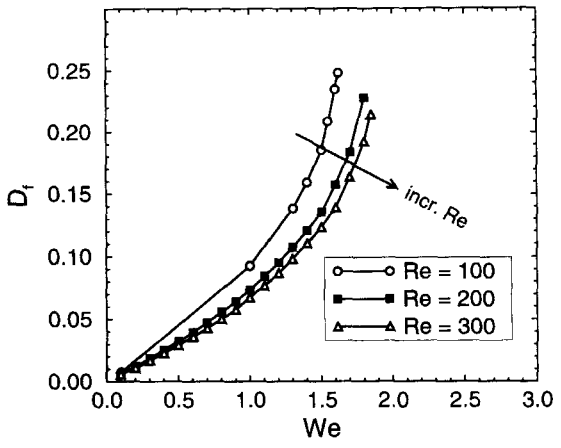

Figure 6. Deformation vs Weber number at $\lambda = \zeta = 1$ for three different Reynolds numbers; ⊙ Re = 100, ■ Re = 200, △ Re = 300.

pressure distribution thus tends to counteract the tendency identified by Ryskin and Leal (1984b) for the case $\zeta = 0$, of the dynamic pressure distribution in the outer fluid to produce a 'barrel' or truncated cylinder. With increase of ζ, the inner fluid pushes the interface in the opposite direction—i.e outward at the ends of the drop and at the equator. The increase in maximum deformation prior to loss of steady solutions, is partially due to the increase of dynamic pressure pushing outward at the ends of the drop, and partly due to the fact that the dynamic pressure maximum at the equator tends to maintain a concave shape and thus delays the formation of a waist.

These qualitative effects of increased density ratio become even more evident as ζ is increased to large values. At $\zeta = 8$ and 20, for example, one can actually see an outward bulge at the equator of the drop.

A number of drop shapes are also shown in figure 5 for $\lambda = 10$. However, the influence of λ, though modest in magnitude, is quite complex. For low values of ζ, increase of λ is seen to produce an increase of deformation. On the other hand, the cases shown in figure 5, indicated that this trend is reversed for larger ζ values. In view of the apparent complexity in behavior, we will postpone discussion on the effects of λ to a point where we display more quantitative data.

We now turn to a more quantitative presentation of the numerically generated data, presented primarily in the form of the scalar deformation parameter, D_f, plotted as a function of the various independent parameters, Re, We, ζ and λ.

We begin in figure 6, with the effects of Reynolds number on deformation for $\zeta = \lambda = 1$. At the upper ends, these deformation curves all show increased sensitivity to changes in We, and our prior study of the limiting case $\lambda = \zeta = 0$ suggests strongly that this is because we are approaching a limit point in We, beyond which steady deformed shapes do not exist. Clearly, the effect of increased Reynolds number is to *decrease* the degree of deformation at fixed We and thus to stabilize the drop in the sense that the critical We for existence of steady solutions is increased. For Re = 100, 200 and 300, respectively, we estimate the critical Weber numbers to be 1.64, 1.85 and 1.9. the critical value for a bubble ($\lambda = \zeta = 0$) at Re = 100, was shown by Ryskin and Leal (1984b) to be 2.1.

Although the effects of an *increase* in ζ appear to be relatively straightforward, leading in every case to modified shapes with an increase in the degree of elongation of the drop (and thus D_f) and a tendency to bulge outward at the equator, effect of λ on the deformation is not at all straightforward. We show (figure 7) the influence of λ on the drop deformation for several different values of the density ratio at a given We = 1.0 and Re = 100. Clearly, the influence of λ is strongly related to the value of ζ. For $\zeta = 2$, when the stagnation pressures in the internal and external fluids are perfectly balanced, the deformation is due solely to viscous stresses and it increases with increase of λ. This trend is also seen for $\zeta = 1$, and is qualitatively similar to the well-known result (Stone and Leal 1989) that the degree of steady deformation increases slightly with increase of the viscosity

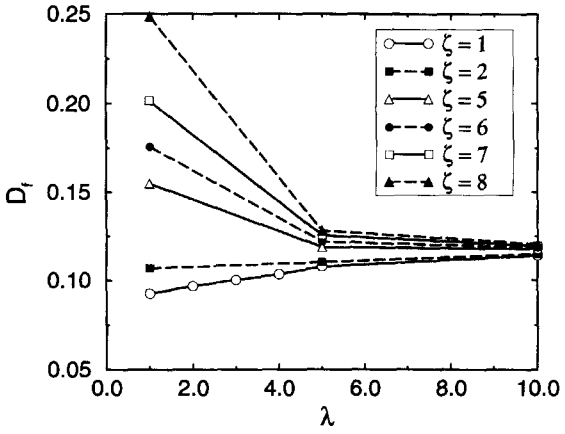

Figure 7. Deformation vs viscosity ratio at Re = 100, We = 1, and several fixed values of ζ; ○ $\zeta = 1$, ■ $\zeta = 2$, △ $\zeta = 5$, ● $\zeta = 6$, □ $\zeta = 7$, ▲ $\zeta = 8$.

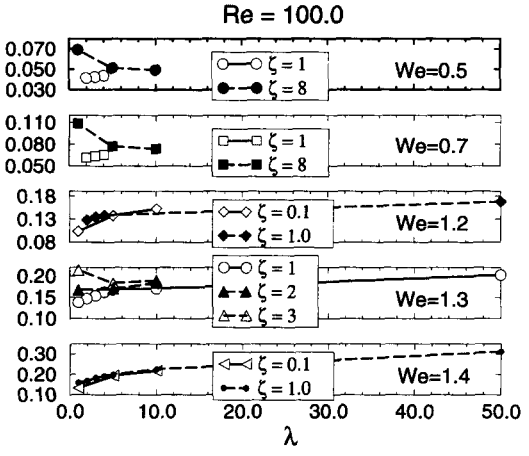

Figure 8. Deformation vs viscosity ratio at Re = 100 and several Weber numbers $0.5 \leqslant We \leqslant 1.4$.

ratio for viscous dominated flows. We see, on the other hand, that the deformation actually *decreases* with increase of λ for $\zeta \geqslant 5$—exactly the opposite trend—and this is a much stronger effect. The same trend was also found at higher Re and We numbers. For example, we consider five other values of We in figure 8. In all cases, D_f decreases with increase of λ for the larger ζ values, but increases for $\zeta \geqslant 2$. Similar results for Re = 200 and 300 are shown in figure 9 for $\zeta = 1$. At fixed We, the sensitivity of D_f to changes in λ is decreased as Re is increased. This latter

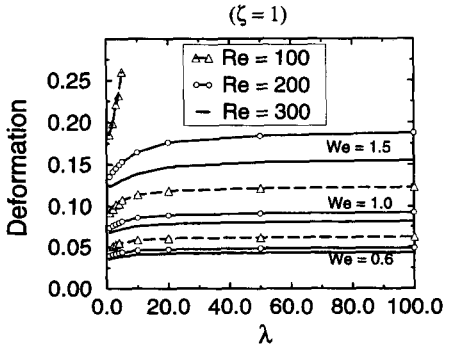

Figure 9. Deformation vs viscosity ratio for $\zeta = 1$, and Re = 100, 200 and 300. Results are shown for each Reynolds number at three different values of We = 0.6, 1.0 and 1.5.

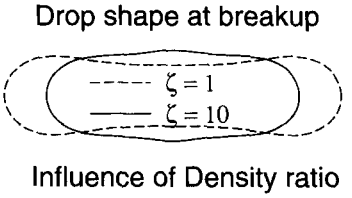

Figure 10. An instantaneous snapshot of drop shapes during transient deformation; $\zeta = 1$, Re = 100, We = 1.64, $\lambda = 1$; and $\zeta = 10$, Re = 100, We = 1.64, $\lambda = 1$.

observation is essentially a consequence of the fact that the critical We is larger for Re = 300 than for Re = 200, so that We is close to the critical value for Re = 200.

Although the effect of λ on shape for $\lambda = O(1)$ is generally modest, it is clear that even small changes in the viscous stresses can have a large effect on deformation for We values that are close to the limit point (cf. figure 6). In this region, the increase of deformation with increase of λ could be expected to cause the drop to become unstable (i.e. to pass beyond the limit point for existence of steady solutions). An example of this is shown in figure 9 for the case Re = 100, $\zeta = 1$ and We = 1.5, which is very near to the limit point for $\lambda = 1$ of We = 1.63. Unlike the other cases shown in figure 9, the results for We = 1.5 and Re = 100 do not plateau with increase of λ. In fact, steady solutions do not exist above $\lambda = 5$ at this Reynolds and Weber number combination. As expected, an increase in λ for $\lambda = O(1)$ has the effect of lowering the critical We for 'breakup'.

The transition from deformation which *increases* slightly with increased λ for $\zeta = O(1)$, to deformation that decreases with increased λ for $\zeta > O(1)$, reflects a transition from deformation due primarily to viscous effects for $\zeta = O(1)$, deformation dominated by the dynamic pressure distribution for $\zeta > O(1)$. As noted previously, the increase in D_f with increase of λ is a feature common to all cases where viscous contributions to the normal stress balance are dominant (also characteristic, for example, of low Reynolds numbers). When $\zeta = 0(1)$, the dynamic pressure contributions from outside and inside the drop essentially cancel, and the increase of deformation with λ is ultimately due to an increased *imbalance* of viscous stress contributions to the normal stress balance.

When $\zeta > O(1)$, the internal and external stagnation pressure contributions to the normal stress balance do not cancel each other out, and for ζ sufficiently large, these dynamic pressure contributions become dominant over the viscous contributions in the normal stress balance provided only that the Reynolds number is sufficiently large (*note*: the necessary value of ζ for this to occur, decreases as Re increases and the relative strength of the two viscous stress contributions is reduced). As we observed earlier, an increase in ζ (with We, λ constant) serves to *increase* the drop deformation as measured by D_f. However, the influence of ζ is coupled to the strength of the internal circulation, and this *decreases* with increase of λ. Since increased dynamic pressure contributions from the inner fluid deform the drop in a way that leads to increased values of D_f, whereas a relative increase in the contributions from the outer fluid has the opposite effect, we find that for 'large' ζ values, the drop is less deformed (i.e. D_f decreases) with increase of λ.

4. DISCUSSION

There are several aspects of this problem that are worth some additional discussion. The first is the mode of transient deformation (and presumably breakup) that ensures once the limiting value of We is reached for the existence of steady solutions. In the case of bubbles (or drops with small ζ and λ), the loss of steady solutions occurs because of the formation of a waist at the center plane of symmetry. In the case of drops with density ratios greater than one, this mode of breakup is not present. Instead, the onset of breakup seems to be related to the extent of the deformation. Figure 10 shows an instantaneous snapshot of *transient* drop shapes for We higher than the critical We for $\zeta = 1$ and $\zeta = 10$. It can be seen that the two transient deformation modes are quite different. For $\zeta > 1$, there is no formation of a waist at the central symmetry plane. However, there is a change in sign of the curvature away from the center that seems to initiate the breakup of the drop.

A second issue of some interest is the extent to which the present results, obtained for Re up to 300, demonstrate a transition to high Reynolds number *asymptotic* behavior. We should first note that the only existing high Reynolds number asymptotic solution for the motion of a drop in a viscous fluid, so far as we are aware, is the solution of Harper and Moore (Harper and Moore 1968) for the buoyancy driven translation of a *spherical* drop through an otherwise quiescent fluid. However, we can anticipate from their solution that the high Reynolds number structure in the present case should consist of a potential flow solution for the deformed drop in the outer fluid, an inviscid solution for the pair of recirculating toroidal zones or the inner fluid; with boundary layers at the drop surface, along the symmetry axis, and along the central symmetry plane inside. The issue is what, if anything, we can say based upon this qualitative picture of the asymptotic flow structure, about the expected shape of the drop in the limit as $\mathrm{Re} \to \infty$. The simplest case is $\zeta = 1$. In that case, if the tangential velocity components in the inviscid flow to the two sides of the boundary-layer at the drop surface were equal, the internal and external dynamic pressure contributions to the normal stress would balance and, in the limit $\mathrm{Re} \to \infty$, the shape would be a sphere, independent of We. In fact, for the translating bubble problem, Harper and Moore 1968 were able to show that the circulation inside a spherical drop differs from the value obtained for a fully inviscid analysis by only an asymptotically small correction

$$\frac{\text{actual}}{\text{inviscid}} = 1 - \frac{f(\lambda, \lambda\zeta)}{\sqrt{\mathrm{Re}}}.$$

Since the inviscid solution for a sphere, namely the Hill's spherical vortex, exactly satisfies the condition of equal tangential velocity across the interface, it follows that the spherical shape is a solution at $\zeta = 1$ for all We provided that Re is large enough for the Harper and Moore (1968) analysis to be valid, namely

$$\frac{\mathrm{Re}}{\lambda^2} \gg 1.$$

It may be noted that this latter condition is even more conservative than the obvious requirement that both the outer and inner Reynolds numbers be large which, for $\zeta = 1$, requires

$$\mathrm{Re} \gg 1, \quad \mathrm{Re}/\lambda \gg 1.$$

Now, it is of interest to examine the solutions obtained in the present study to see whether they show evidence of asymptotic behavior at the largest Reynolds numbers which is consistent with this picture. If we return to figure 6, which shows calculated results for the deformation parameter, D_f vs We for $\zeta = 1$, there seems to be some convergence of results with increase of Re, but no evidence of any transition toward the result $D_f \equiv 0$ for all We that would be inferred from the preceding discussion as representing the $\mathrm{Re} \to \infty$ limiting behavior. One possibility is that $\mathrm{Re} = 300$ is simply not large enough. It is perhaps worth noting in this respect that the analysis of Harper and Moore (1968) would require a Reynolds number of 3×10^4 for $\lambda = 1$ and $\zeta = 1$ to yield a viscous correction of less than 5% in the internal circulation, and much larger values for $\lambda \geqslant 1$. Another possible explanation is that the solution corresponding to $D_f \equiv 0$ for all We is *not unique*, and that the result for $\mathrm{Re} = 300$ is actually a reasonable qualitative indicator of the expected behavior for $\mathrm{Re} \to \infty$ on a second branch of steady solutions that evolves from $D_f = 0$ for $\mathrm{We} \equiv 0$. It is, in fact, likely that the solution branch $D_f = 0$ cannot be reached by simply increasing Re from an initial state that is non-spherical. Harper (1972) has already pointed out, in the case of the translating drop, that a sphere is the only shape for which an inviscid solution can be found that has a continuous tangential velocity across the interface at all points. Hence, we may expect an imbalance of the dynamic pressures even for $\zeta = 1$ for any shape that is not spherical and this suggests the possibility of a solution branch with finite deformation even for $\mathrm{Re} \to \infty$. With the solutions that we have, we are not able to distinguish between these possible explanations of the difference between the behavior in figure 6, and that inferred from the Harper and Moore (1968) analysis of a translating *spherical* bubble.

One final point for discussion is the fact that we have discovered a purely empirical correlation for the high Reynolds number cases (100–300) that does a very good job of reducing all of the results for the shape at various values of λ and ζ to a simple curve. This correlation is based upon

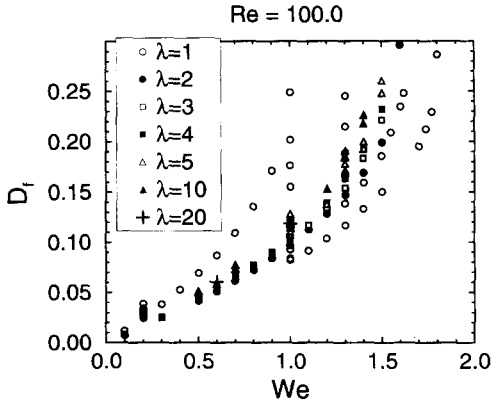

Figure 11. Deformation vs Weber number at Re = 100, for all values of ζ, and for $\lambda \leqslant 20$.

the following observations. First, based upon the deformation measure, D_f, *increases* in the density ratio are found to produce an increase in deformation. Second, except for a small range of ζ values near unity, where the shape is relatively insensitive to λ (cf. figure 7), increases in λ are found to produce a decrease in D_f, at least up to $\lambda \sim O(10)$, beyond which the shape becomes insensitive to λ (cf. figure 7 or figure 8). We can think of these changes as suggesting that increases in ζ or decreases in λ are equivalent to subjecting the drop to a higher Weber number. The simplest suggestion for data correlation that is consistent with this notion is to plot D_f vs a modified or rescaled Weber number, i.e.

$$\mathrm{We}^* = \mathrm{We}\left[1 + c\frac{(\zeta - 1)}{\lambda}\right]$$

where we have chosen arbitrarily to use $\zeta = 1$ as our base case. Such a simple form of rescaling cannot be expected to work for $\lambda > O(10)$ because it does not capture the sensitivity of shape to both ζ and λ at large λ. We have also not attempted to deduce any scaling dependence for Re. The result of figure 6 suggest that we do not have numerical data over a significantly wide range of Re values to justify any such scaling.

An example of the applicability of this approach of this proposed rescaling for $\lambda \leqslant 20$ and Re = 100 (where we have numerical data over a wide range of ζ values), can be seen by comparing the results shown in figure 11 for D_f vs We with the results in figure 12 where the same data is plotted vs the rescaled Weber number We* with a value of the coefficient $c = 0.1$. A composite of all available results for Re = 100, 200, 300 and $\lambda \leqslant 10$ is shown in figure 13, again as a function of We* for the same value of c. The spread shown is primarily due to the same Reynolds number dependence that was shown in figure 6.

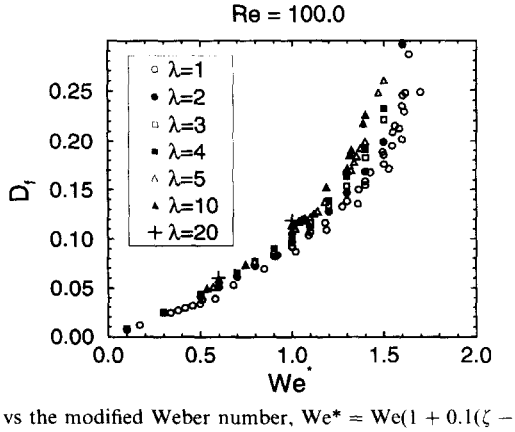

Figure 12. Deformation vs the modified Weber number, We* = We(1 + 0.1(ζ − 1)/λ) for Re = 100 and all values of ζ, and $\lambda \leqslant 20$.

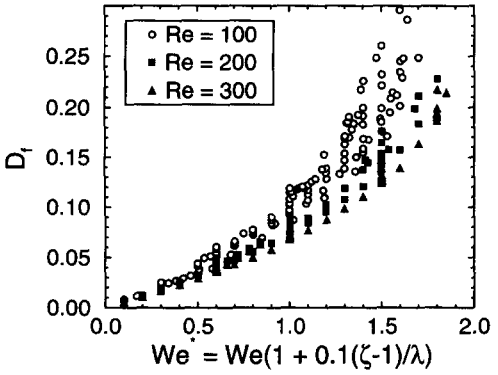

Figure 13. Deformation vs We* for three values of Re = 100, 200 and 300, and all values of ζ, and $\lambda \leqslant 20$. The change observed with Reynolds number is similar to figure 6.

We do not know whether the simple correlation of shapes for this modest range of Reynolds numbers and $\lambda(1 \leqslant \lambda \leqslant 20)$ will find any practical use. However, it clearly does a good job of accounting for variations in ζ and λ. We have attempted to provide a more rational explanation, based upon ideas about the expected asymptotic solution structure for large Re, but have been unsuccessful and probably should not be surprised by this in view of the likelihood (stated earlier) that Re = 300 is much too low to exhibit limiting behavior.

Acknowledgements—This work was supported by a grant from the fluid mechanics program of the National Science Foundation, and by a grant for computing resources from the SDSC. We also wish to thank Prof. J. F. Harper for an illuminating discussion about the asymptotic nature of the problem for large Reynolds number.

REFERENCES

Barmatz, M. (1982) *Materials Processing in Reduced Gravity Environment of Space*, p. 25. North-Holland, Amsterdam.

Dandy, D. S. and Leal, L. G. (1989) Buoyancy-driven motion of a deformable drop through a quiescent liquid at intermediate Reynolds numbers. *J. Fluid Mech* **208,** 161–192.

Doremus, R. H. and Nordine, P. C., eds (1986) Materials processing in the reduced gravity environment of space. *Materials Research Society Symposia Proceedings*, Vol. 95. Materials Research Society Boston, MA, U.S.A.

Harper, J. F. (1972) The motion of bubbles and drops through liquids. *Advances in Applied Mechanics* **12,** 59–129.

Harper, J. F. and Moore, D. W. (1968) The motion of a spherical liquid drop at high Reynolds number. *J. Fluid Mech.* **32,** 367–391.

Kang, I. S. and Leal, L. G. (1987) Numerical solution of axisymmetric, unsteady free-boundary problems at finite Reynolds number. I. Finite-difference scheme and its application to the deformation of a bubble in uniaxial straining flow. *Phys. Fluids A* **30,** 1929–1940.

Kang, I. S. and Leal, L. G. (1989) Numerical solution of axisymmetric, unsteady free-boundary problems at finite Reynolds number. II. Deformation of a bubble in biaxial straining flow. *Phys. Fluids A* **32,** 644–660.

Koh, C. J. and Leal, L. (1972) The stability of drop shapes for translation at zero Reynolds numbers through a quiescent fluid. *Advances in Applied Mechanics* **12,** 59–129.

Lai, C. L. (1990) Unsteady thermo capillary flows and free surface oscillations in reduced gravity environments. *Acta Astronautica* **21,** 171–181.

Ryskin, G. and Leal, L. G. (1983) *J. Computational Physics* **50,** 71.

Ryskin, G. and Leal, L. G. (1984a) Numerical solution of free-boundary problems in fluid mechanics. Part 1. The finite-difference technique. *J. Fluid Mech.* **148,** 1–17.

Ryskin, G. and Leal, L. G. (1984b) Numerical solution of free-boundary problems in fluid

mechanics. Part 3. Bubble deformation in an axisymmetric straining flow. *J. Fluid Mech.* **148,** 37–43.

Stone, H. A. and Leal, L. G. (1989) Relaxation and breakup of an initially extended drop in an otherwise quiescent fluid. *J. Fluid Mech.* **198,** 399–427.

Wozniak, G. (1991) On the thermocapillary motion of droplets under reduced gravity. *Journal of Colloid and Interface Science* **141,** 245–254.